PAPER

Check for updates

Preparation of SiO₂ nanowire arrays as anode material with enhanced lithium storage performance

Wen Li, Fan Wang, Mengnan Ma, Junshuang Zhou, Yuwen Liu and Yan Chen ⓘ *

SiO₂ nanowire arrays have been prepared by a template-assisted sol gel method and used as a negative electrode material for lithium ion batteries. Amorphous SiO₂ was confirmed by X-ray diffraction and Fourier transform infrared spectroscopy. The results of scanning electron microscopy and transmission electron microscopy confirmed that the SiO₂ nanowire had a diameter of about 100 nm and a length of about 30 μm. Cyclic voltammetry and constant current charge and discharge tests showed the prepared SiO₂ nanowire arrays were electrochemically active at a potential range of 0.05–3.0 V. At a current density of 200 mA g⁻¹, the first discharge specific capacity was as high as 2252.6 mA h g⁻¹ with a coulombic efficiency of 60.7%. Even after about 400 cycles, it still maintained 97.5% of the initial specific capacity. Moreover, a high specific capacity of 315 mA h g⁻¹ was exhibited when the current density was increased to 2500 mA g⁻¹. SiO₂ nanowire array electrodes with high reversible capacity and good cycle performance provide potential anode materials for future lithium-ion batteries.

1. Introduction

Lithium-ion batteries have been widely used as the main source of power for various portable electronic devices due to their high energy density, long cycle life, lack of memory effect and environmental friendliness.[1–4] Owing to the traditional graphite-based anodes having limited capacity (theoretical capacity: 372 mA h g⁻¹),[5–7] lots of work has focused on the development of electrode materials for lithium-ion batteries. In recent years, as lithium storage materials for lithium batteries, many oxide anode materials have been extensively studied.[8–12] Since $Li_{22}Si_5$ corresponds to the highest known theoretical capacity of 4200 mA h g⁻¹, it is more concerned about Si materials and is considered to be the best anode material for next-generation lithium-ion batteries.[13–18] For example, Demirkan et al. reported that the capacity of a silicon anode for LIB was 2320 mA h g⁻¹.[19] Hwa et al. synthesized Si by chemical vapor deposition and reported a capacity of 1600 mA h g⁻¹.[20] Although silicon has a high theoretical capacity, its volume change is as high as 300%, resulting in pulverization of Si particles and electrical contact loss during charge/discharge (alloying/de-alloying). This causes a rapid reduction in capacity and limits the commercial application of LIB.[21–23]

As an alternative, SiO₂ has similar advantages to Si, such as: high Li storage capacity (theoretical specific capacity is 1965 mA h g⁻¹), low discharge potential.[24] In addition, it is abundant in storage, environmentally friendly, low cost and easy to prepare on the earth, making it an important anode material.[25–27] Moreover, compared with Si, the volume change of SiO₂ is much smaller, and it has better cycle stability. When SiO₂ is used as negative electrode materials for lithium ion batteries, bulk crystal SiO₂ is generally considered to be not electrochemically active due to its strong Si–O bond and poor conductivity.[25,28] However, it has been reported that nano-SiO₂ exhibits Li reactivity in an amorphous state. To date, a large amount of research work has been devoted to the reversible lithium storage behavior of SiO₂ anodes through its morphology and crystallinity control. For example, SiO₂ film,[29] SiO₂ tube,[30] hollow porous SiO₂ nanocube,[31] SiO₂ nanosphere[32] and SiO₂–C nanomixture,[33–39] etc.

In this study, SiO₂ nanowire arrays were prepared by means of sol–gel methods to assist AAO templates. The method is simple, environmentally friendly, and the morphology of the SiO₂ nanowire is controllable. When it was used as a negative electrode material for a lithium ion battery, it had a high aspect ratio and increased a specific surface area. Therefore, the diffusion path of lithium ions was reduced, thereby increasing the diffusion ability of lithium ions. In addition, the nano-sized SiO₂ electrode material can provide mechanical strain during cycling to alleviate the problem of severe cracking and pulverization of the electrode material due to large volume changes during alloying/de-alloying with Li. The SiO₂ nanowire arrays exhibit remarkable lithium storage capacity in terms of high specific capacity, excellent cycle performance and high rate capacity.

Hebei Key Laboratory of Applied Chemistry, College of Environmental and Chemical Engineering, Yanshan University, Qinhuangdao, Hebei 066004, China. E-mail: chenyan@ysu.edu.cn; Tel: +86-335-8061569

2. Experimental

2.1 Preparation of SiO₂ nanowire arrays

4 g of tetraethyl orthosilicate (TEOS) was slowly added to 9.6 ml of absolute ethanol to form a TEOS solution. Then, 9.6 ml of absolute ethanol was mixed with 1.5 g of water and 0.02 g of HCl. Finally, the second solution was slowly added dropwise to the TEOS solution while stirring on a magnetic stirrer for 3 h to obtain silica sol at room temperature.

An anodized aluminum oxide template having a thickness of about 30 μm and a pore diameter of about 100 nm was prepared by a two-step anodization method in a 0.3 mol L⁻¹ oxalic acid solution, and subjected to subsequent treatment to obtain a two-pass template. First, the AAO template was immersed in the prepared silica sol for 24 hours at room temperature, and ultrasonic waves were assisted for 1–3 minutes from the start of soaking to remove bubbles in the AAO template. During this process, the sol enters the template pore by capillary action. After the soaking was completed, the template was taken out and washed with deionized water and naturally dried. Then, the SiO₂ nanowire arrays-AAO template was adhered to the copper foil substrate with a conductive silver paste. After drying at 125 °C for 45 minutes, the SiO₂ nanowire arrays-AAO template-copper foil was immersed in 15% dilute hydrochloric acid for 8 hours to dissolve the AAO template, exposing the SiO₂ nanowire arrays. Finally, the specimens were washed with absolute ethanol and deionized water and dried for further experiments.

2.2 Microscopic characterization

The morphology and structure of the product were characterized by transmission electron microscopy (TEM, JEM2010F) and scanning electron microscopy (FE-SEM, Zeiss Supra 55) equipped with an energy dispersive X-ray spectrometer (EDS, Thermo Fisher Scientific, NORAN System 7). X-ray diffraction (XRD) measurements were performed on a RigakuD/MAX 2500/PC diffractometer with Cu Ka radiation (λ = 1.5418 Å). The sweep speed is 5° min⁻¹ and the scan range is 5–90°. Fourier transform infrared (FT-IR) spectra recorded on a Thermo scientific Nicolet 380 Fourier transform spectrometer using a KBr pellet technique were used to characterize the samples.

2.3 Electrochemical measurement

In this study, the SiO₂ nanowire arrays and the copper foil substrate were connected to each other by a conductive silver paste to prepare an electrode material, so that it is not necessary to add a conductive agent and a binder for smearing. The mass of the active material (SiO₂ nanowire arrays) on the electrode obtained by weighing was 0.3 mg. Alternatively, the total mass can also be determined by determining the number of nanowires based on the pore density of the AAO template followed through the diameter and length of the nanowires. Finally, the mass of the active substance was determined to be 0.3 mg. After the electrode material was dried in a vacuum oven at 80 °C for 12 hours, it could be directly used as a negative electrode material in a lithium ion battery for electrochemical performance testing. Li foil was used as the positive electrode of the

battery. The electrolyte was 1 M LiPF₆ dissolved in ethylene carbonate (EC)/dimethyl carbonate (DMC)/ethyl methyl carbonate (EMC) in a volume ratio of 1 : 1 : 1. The battery was assembled in an Ar-filled glove box. Finally, the cell was aged for 12 hours before further electrochemical measurements.

Constant current cycle measurements were performed at constant temperature using the Land CT 2001A battery test system. The cut-off potential window for the constant current charge and discharge test was 3.0 and 0.05 V (vs. Li/Li⁺). Cyclic voltammetry (CV) was recorded on a CHI660E electrochemical workstation with a potential range of 0.0–3.0 V and a scan rate of 0.1 mV s⁻¹. All electrochemical measurements were made at 25 °C.

3. Results and discussion

3.1 Morphological and structural analysis of SiO₂ nanowire arrays

The composition of the obtained sample was confirmed by XRD and FTIR, respectively. The XRD pattern of the material (Fig. 1a) showed a single broad peak at about 23° which proved to be amorphous SiO₂ according to the standard pattern of JCPDS PDF #029-0085. In the FTIR spectrum (Fig. 1b), the bands at 1075 cm⁻¹ and 800 cm⁻¹ illustrated the asymmetric tensile vibration of Si–O–Si and the symmetric tensile vibration of Si–O–Si, respectively. The band vibration of SiO₂ at 469 cm⁻¹ was the third characteristic peak of amorphous silica.[40] XRD and FTIR results indicated that the sample heated at 125 °C was amorphous SiO₂. The XPS test was used to further confirm the composition of the sample as shown in Fig. 1c. The Si 2p spectrum showed a peak at about 103.4 eV, indicating that Si exists in the state of SiO₂.

The morphology and composition of the prepared SiO₂ nanowire arrays were investigated by scanning electron microscopy (SEM) and energy dispersive spectroscopy (EDS). Fig. 2a–d are the microscopic morphology of the SiO₂ nanowire arrays at different magnifications. They can be clearly seen that the SiO₂ nanowire arrays after removing the AAO template adhere well to the copper foil substrate. The nanowires grow evenly, densely and orderly, with no obvious defects on the surface, and the aspect ratio is as high as 300 : 1. They are about 30 μm in length and about 100 nm in diameter, which is consistent with the thickness and pore size of the AAO template. In addition, it is seen in Fig. 2b that the SiO₂ nanowire arrays exhibit a certain degree of lodging due to the loss of support of the AAO template and the high aspect ratio of the nanowire itself. Fig. 2e is the EDS characterization of the nanowires. As can be seen from the figure, the composition of the nanowire is Si and O, and the weight percentage of the two is close to 1 : 2. The reason for the high O content may be due to the strong surface activity of the nano SiO₂, which is easy to adsorb water in the air, as well as chemically bound water. The selected area EDS mapping was performed on the area within the red frame of Fig. 2e to evaluate the distribution uniformity of O and Si in the SiO₂ nanowires. It can be clearly seen in Fig. 2g, h that O and Si are uniformly distributed in the material.
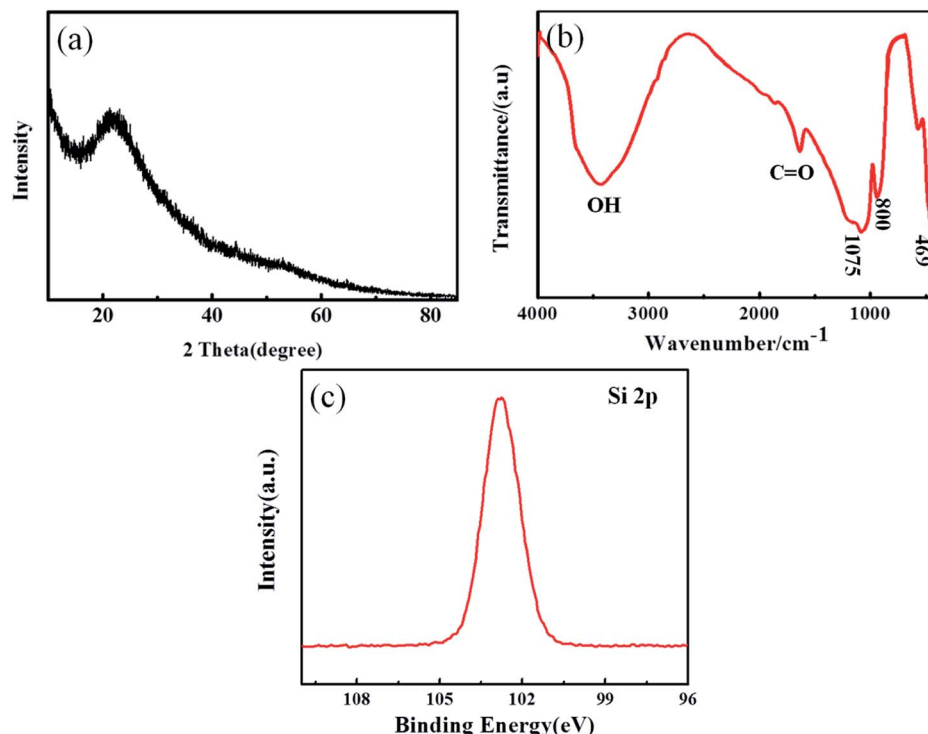
Fig. 1 XRD pattern (a), FTIR spectrum (b) and XPS spectrum (c) of the as-prepared SiO_2.

Fig. 3 shows a TEM microscopic image of a single SiO_2 nanowire and undispersed nanowires after ultrasonic dispersion. It can be seen that the entire nanowire is smooth and uniform with a diameter of about 100 nm, which is consistent with the SEM image.
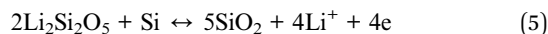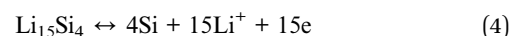
3.2 Electrochemical performance

Further studies of the reaction mechanism and kinetics were carried out in the first three cycles of the CV curve of the SiO_2 nanowire arrays (Fig. 4a). The test was performed at a scan rate of 0.1 mV s^{-1} in a voltage window of 0.05–3.0 V (vs. Li$^+$/Li). It can be found that the CV curve is consistent with the charge and discharge curves, and the two cathode peaks in the initial discharge curve correspond to the platform in Fig. 4b. In the first cycle, there are two obvious reduction peaks nearly located at 1.5 V and 1 V. The peak at 1.5 V contributes to the reductive decomposition of the electrolyte solution and the formation of a solid electrolyte interface (SEI) layer on the anode surface, which is an important cause of the irreversible capacity in the initial discharge.[41] The peak at 1 V indicates some chemical reaction between SiO_2 and Li$^+$. When the material was initially discharged, amorphous SiO_2 was reduced to Si and formed $Li_2Si_2O_5$ or Li_4SiO_4.[42] The irreversible Li_4SiO_4 phase formed in the reaction consumed a large amount of Li$^+$, accounting for another large portion of the irreversible capacity. The responses can be summarized as follows:

Discharge reaction:

$$5SiO_2 + 4Li^+ + 4e \leftrightarrow 2Li_2Si_2O_5 + Si \quad (1)$$

$$2SiO_2 + 4Li^+ + 4e \rightarrow Li_4SiO_4 + Si \quad (2)$$

$$4Si + 15Li^+ + 15e \leftrightarrow Li_{15}Si_4 \quad (3)$$

During the initial charge cycle, a prominent peak at about 0.1 V should be associated with the reversible alloy/de-alloy reaction with Li$^+$, which makes the contribution to lithium storage capacity. During the subsequent scan cycles, the CV curves became stable, corresponding to the reversible behavior to some extent. Similar CV behavior indicates that nano-SiO_2 materials are also electrically active for lithium storage. The results are similar to the previous literature.[14,29] During charging, the reactions can be summarized as follows:

Charging reaction:

$$Li_{15}Si_4 \leftrightarrow 4Si + 15Li^+ + 15e \quad (4)$$

$$2Li_2Si_2O_5 + Si \leftrightarrow 5SiO_2 + 4Li^+ + 4e \quad (5)$$

Since the prepared SiO_2 nanowire arrays negative electrode material and the half-cell composed of the lithium metal counter electrode showed good redox characteristics, the charge–discharge voltage profiles of the different cycles were performed at a current density of 200 mA g^{-1} in a voltage range of 0.05–3.0 V (as shown in Fig. 4b). There is a distinct platform at about 1.5 V in the first lithiation curve, which is in full compliance with the first CV curve. As observed from the cyclic performance in Fig. 4a, the SiO_2 anode delivered an initial discharge capacity of 2252.6 mA h g^{-1} and a charge capacity of 1368 mA h g^{-1}, with an initial coulombic efficiency of 60.7%.
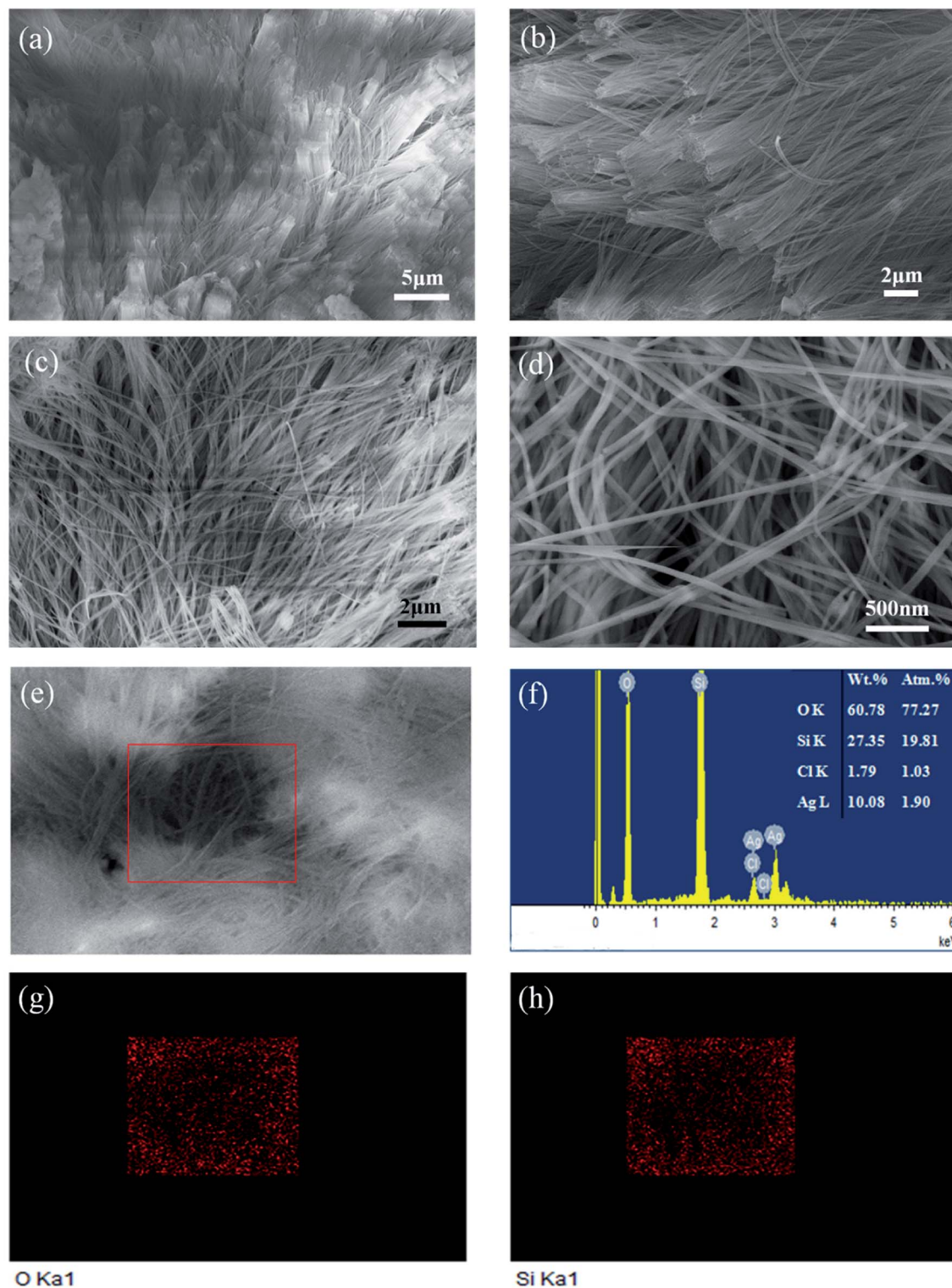
Fig. 2   SEM image of SiO$_2$ nanowire arrays (a–e). EDS spectroscopy and quantitative analysis of SiO$_2$ nanowires (f). EDS microanalysis of element Si and O for selected region (g and h).

The initial irreversible capacity loss is mainly due to the formation of the solid electrolyte interphase (SEI) layer and the irreversible reaction of SiO$_2$ with Li ions and electrolyte decomposition.

The cyclic performance of the SiO$_2$ nanowire arrays electrode was tested at a current density of 200 mA g^{-1} with the voltage window of 0.05–3 V, and the result is plotted in Fig. 4c. Although the electrode showed a large initial irreversible capacity, it was
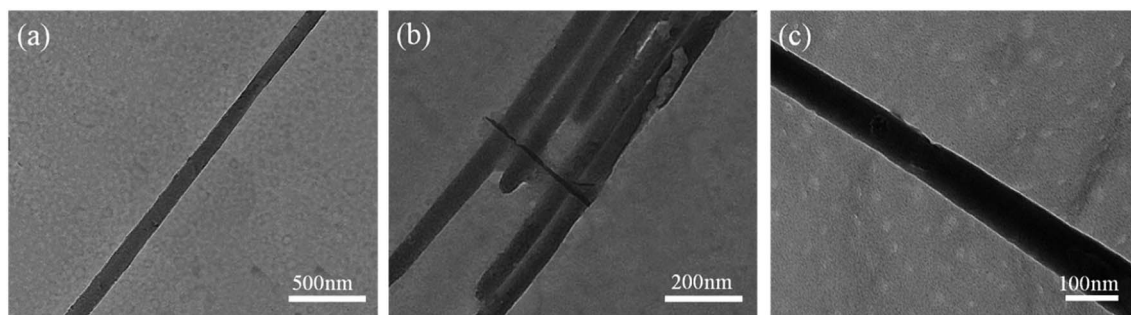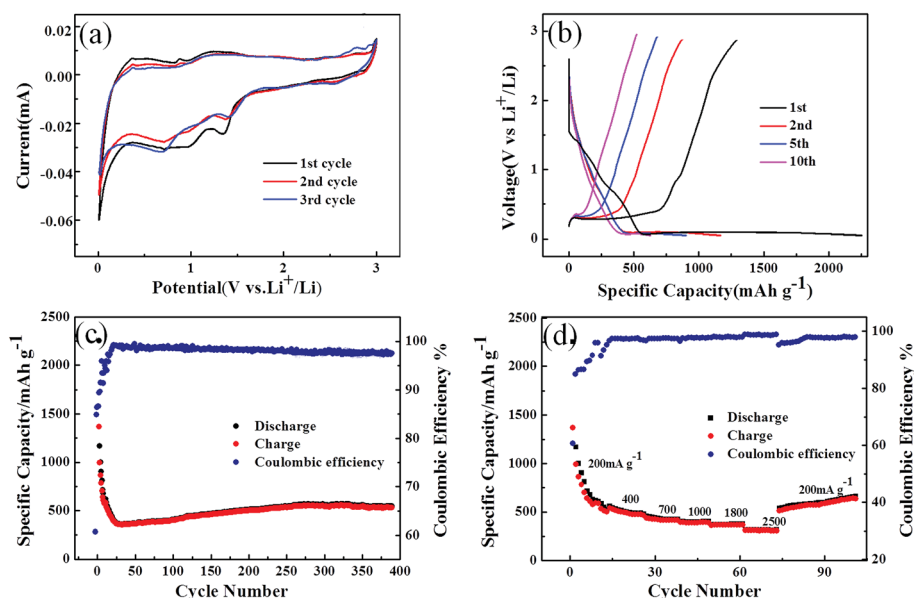
Fig. 3 TEM images of the SiO$_2$ nanowires.

Fig. 4 (a) Cyclic voltammetry of SiO$_2$ nanowire arrays between 3 and 0 V at a scan rate of 0.1 mV s^{-1}. (b) The charge–discharge profiles for different cycles. (c) Cycling performance and coulombic efficiency of SiO$_2$ nanowire arrays electrode under 200 mA g^{-1} within a voltage of 0.05–3.0 V. (d) Rate performance of SiO$_2$ nanowire arrays electrode.

found to remain at about 545.4 mA h g^{-1} even above 400 cycles, and the coulombic efficiency was higher than 97.5%. It is worth noting that the specific capacity of the SiO$_2$ anode was reduced in the first few cycles due to the formation of the SEI layer and the insufficient utilization of SiO$_2$ in the initial cycle. Then after about 20 cycles, the specific capacity began to increase

gradually. This is because the gradual increase in the Si phase during the late lithiation–delithiation cycle,[44,45] and the Li$_4$SiO$_4$ matrix formed by the reaction 2 alleviate the volume expansion during the cycle. Therefore, as shown in Fig. 4c, the specific capacity first decreases and then rises again, and continues to maintain equilibrium after about 280 turns.
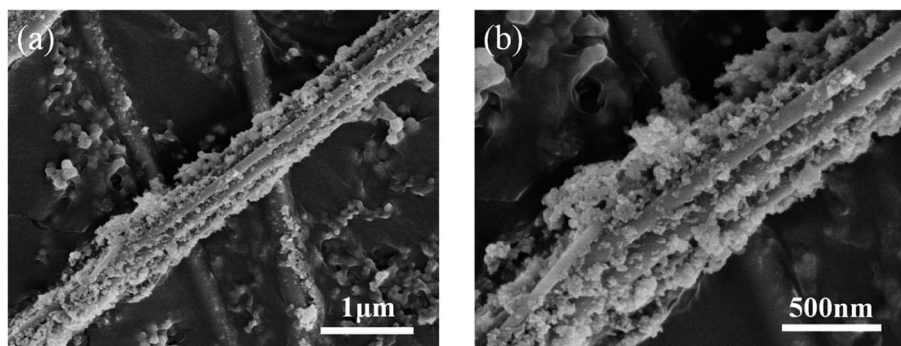

Fig. 5 SEM images of SiO$_2$ electrode after 400 cycles at a current density of 200 mA g^{-1}.

Table 1 Comparison of the lithium-storage performance between this work and reported SiO_2-based anode materials previously

Materials	Current density	Initial discharge specific capacity (mA h g^{-1})/coulombic efficiency (%)	Reversible capacity (mA h g^{-1})/cycle number (n)	Rate performance (higher current density)/specific capacity (mA h g^{-1})	Ref.
Nanostructured SiO_2	7 mA g^{-1}	270/47	ca. 120/50	100 mA g^{-1}/80	43
SiO_2 nanobelts	100 mA g^{-1}	1723/50	1012/100	1000 mA g^{-1}/574	46
Hollow porous SiO_2 nanocubes	100 mA g^{-1}	3084/47	919/30	—	31
SiO_2 thin film	28 µA cm^{-2}	539/71	510/100	—	29
SiO_2 nanotubes	100 mA g^{-1}	1040/43.3	1266/100	400 mA g^{-1}/814	30
SiO_2 nanospheres	0.1 C	2420/44	876/100	2 C/1085	14
Multi-shell hollow SiO_2 microspheres	100 mA g^{-1}	792.5/53.9	750/550	2400 mA g^{-1}/95	47
SiO_2 nanowire arrays	200 mA g^{-1}	2252.6/60.7	545.4/400	2500 mA g^{-1}/315	This work

To evaluate the rate-ability of the sample SiO_2 nanowire arrays, a stepped cycle test was performed at different current densities. The results are shown in Fig. 4d. The battery was first cycled at a rate of 200 mA g^{-1} and then successfully switched to 200, 400, 700, 1000, 1800, 2500 mA g^{-1}. It can be seen that the material exhibited a decreasing specific capacity during the first 10 cycles of the initial cycle (200 mA g^{-1}) due to the formation of the SEI layer. However, as can be know from Fig. 4c, the specific capacity gradually increased and stabilized in the subsequent cycle, reaching 545.4 mA h g^{-1}. As the current density increased, the reversible capacity decreased slightly. When the current density increased to 2500 mA g^{-1}, the SiO_2 nanowire arrays electrode can still provide a reversible capacity of about 315 mA h g^{-1} with a coulombic efficiency of 99%. As can be seen in Fig. 4d, when the current density was converted from 2500 to 200 mA g^{-1}, the specific capacity can reach about 659 mA h g^{-1} in the first 30 cycles, with the coulombic efficiency is 98% and in a state of increasing. It is proved that the electrode has good structural stability and excellent rate performance. This is related to the high surface area of the SiO_2 nanowires, which can reduce the diffusion path of lithium ions and enhance their diffusion ability. Based on the above discussion, it can be considered that the SiO_2 nanowire arrays are promising anode material that can improve the electrochemical performance of LIB.

Fig. 5 shows the morphology and structure of SiO_2 nanowire arrays electrode after 400 lithiation–delithiation cycles at 200 mA g^{-1} current densities. Compared with Fig. 2d, it can be seen that after a series of reactions of SiO_2 nanowires with Li$^+$, the nanowires showed a certain degree of volume expansion, but the nanowires morphology does not appear to be severely broken. The results further demonstrate that the SiO_2 nanowire arrays electrode has excellent cycle performance.

Compared with the SiO_2 electrode synthesized by other methods, the SiO_2 nanowire arrays electrode material exhibits superior electrochemical performance. The specific contents are shown in Table 1 below. However, in general, the conductivity of SiO_2 is relatively low, resulting in fewer electronically conductive channels and lower utilization of active materials in the electrodes. Meanwhile, the problem that the volume expansion of the material during charging and discharging causes the active material to fall off has a great influence on electrochemical performance. Based on the above problems, work is under progress to improve the electrochemical performance of the battery by coating the prepared SiO_2 nanowires with conductive materials such as a conductive polymer.

4. Conclusion

In summary, the SiO_2 nanowire arrays were successfully prepared by alumina template assisted sol–gel method, and the average diameter of the nanowire was 100 nm as well as about 30 µm in length. At a current density of 200 mA g^{-1}, an initial discharge capacity was up to 2252.6 mA h g^{-1} and a charge capacity was 1368 mA h g^{-1} with the initial coulombic efficiency of 60.7%. The specific capacity of 545.4 mA h g^{-1} was maintained after about 400 cycles and the coulombic efficiency was

maintained at 97.5%. Especially, when the current density is increased to 2500 mA g^{-1} and then back to 200 mA g^{-1}, the specific capacity can reach to 659 mA h g^{-1}. Thus, the electrode showed excellent cycle performance and rate performance, which was attribute to the large specific surface area of the SiO$_2$ nanowire arrays reducing the diffusion path of lithium ions and providing sufficient lithium ions to react with the silica. Meanwhile, the Si, Li$_2$O and Li$_4$SiO$_4$ matrices produced during the cycle act as a shielding layer and also improve lithium storage performance.

Conflicts of interest

There are no conflicts to declare.

References

1 M. Armand and J. M. Tarascon, *Nature*, 2008, **451**, 652–657.
2 J. W. Choi and D. Aurbach, *Nat. Rev. Mater.*, 2016, **1**, 16013–16029.
3 G. B. Peter, S. Bruno and T. Jean-Marie, *Angew. Chem., Int. Ed.*, 2008, **47**, 2930–2946.
4 Q. Xiao, M. Gu, H. Yang, B. Li, C. Zhang, Y. Liu, F. Liu, F. Dai, L. Yang and Z. Liu, *Nat. Commun.*, 2015, **6**, 8844–8852.
5 R. Shahid and S. Murugavel, *Mater. Chem. Phys.*, 2013, **140**, 659–664.
6 B. Wang, B. Luo, X. Li and L. Zhi, *Mater. Today*, 2012, **15**, 544–552.
7 B. S. M. Weil, *Rev. Metall.*, 2013, **1**, 65–76.
8 H. Fei, D. Li, W. C. Li, L. Cheng, S. Qiang and A. H. Lu, *Adv. Funct. Mater.*, 2013, **23**, 1692–1700.
9 F. X. Ma, H. Hu, H. B. Wu, C. Y. Xu, Z. Xu, L. Zhen and X. W. Lou, *Adv. Mater.*, 2015, **27**, 4097–4101.
10 P. Sun, C. Wang, J. Liu, X. Zhou, X. Li, X. Hu and G. Lu, *ACS Appl. Mater. Interfaces*, 2015, **7**, 19119–19147.
11 J. Yuan, C. Chen, Y. Hao, X. Zhang, B. Zou, R. Agrawal, C. Wang, H. Yu, X. Zhu and Y. Yu, *J. Alloys Compd.*, 2017, **691**, 34–39.
12 G. Zhang, H. B. Wu, T. Song, U. Paik and X. W. Lou, *Angew. Chem., Int. Ed.*, 2014, **53**, 12590–12593.
13 S. Fang, L. Shen, G. Xu, P. Nie, J. Wang, H. Dou and X. Zhang, *ACS Appl. Mater. Interfaces*, 2014, **6**, 6497–6503.
14 J. Tu, Y. Yuan, P. Zhan, H. Jiao, X. Wang, H. Zhu and S. Jiao, *J. Phys. Chem. C*, 2014, **118**, 7357–7362.
15 H. Wang, Z. Yang, C. Liu, S. Huang, H. Wang, Y. Chen and G. Chen, *Biochem. Biophys. Res. Commun.*, 2014, **454**, 71–77.
16 P. Wu, H. Wang, Y. Tang, Y. Zhou and T. Lu, *ACS Appl. Mater. Interfaces*, 2014, **6**, 3546–3552.
17 L. Xue, K. Fu, Y. Li, G. Xu, Y. Lu, S. Zhang, O. Toprakci and X. Zhang, *Nano Energy*, 2013, **2**, 361–367.
18 L. Xue, G. Xu, Y. Li, S. Li, K. Fu, Q. Shi and X. Zhang, *ACS Appl. Mater. Interfaces*, 2013, **5**, 21–25.
19 M. T. Demirkan, L. Trahey and T. Karabacak, *Thin Solid Films*, 2016, **600**, 126–130.
20 Y. Hwa, W. S. Kim, B. C. Yu, S. H. Hong and H. J. Sohn, *Energy Technol.*, 2013, **1**, 327–331.

21 X. Chen, K. Gerasopoulos, J. Guo, A. Brown, C. Wang, R. Ghodssi and J. N. Culver, *ACS Nano*, 2010, **4**, 5366–5372.
22 L. F. Cui, L. Hu, J. W. Choi and Y. Cui, *ACS Nano*, 2010, **4**, 3671–3678.
23 T. Song, J. Xia, J. H. Lee, D. H. Lee, M. S. Kwon, J. M. Choi, J. Wu, S. K. Doo, H. Chang and W. I. Park, *Nano Lett.*, 2010, **10**, 1710–1716.
24 M. Miyachi, H. Yamamoto, H. Kawai, T. Ohta and M. Shirakata, *J. Electrochem. Soc.*, 2005, **152**, 4803–4837.
25 W. S. Chang, C. M. Park, J. H. Kim, Y. U. Kim, G. Jeong and H. J. Sohn, *Energy Environ. Sci.*, 2012, **5**, 6895–6899.
26 P. Lv, H. Zhao, J. Wang, X. Liu, T. Zhang and Q. Xia, *J. Power Sources*, 2013, **237**, 291–294.
27 D. Nan, J.-G. Wang, Z.-H. Huang, L. Wang, W. Shen and F. Kang, *Electrochem. Commun.*, 2013, **34**, 52–55.
28 P. Lv, H. Zhao, J. Wang, X. Liu, T. Zhang and Q. Xia, *J. Power Sources*, 2013, **237**, 291–294.
29 Q. Sun, B. Zhang and Z.-W. Fu, *Appl. Surf. Sci.*, 2008, **254**, 3774–3779.
30 Z. Favors, W. Wang, H. H. Bay, A. George, M. Ozkan and C. S. Ozkan, *Sci. Rep.*, 2014, **4**, 4605–4612.
31 N. Yan, F. Wang, H. Zhong, Y. Li, Y. Wang, L. Hu and Q. Chen, *Sci. Rep.*, 2013, **3**, 1568–1574.
32 J. Tu, Y. Yuan, P. Zhan, H. Jiao, X. Wang, H. Zhu and S. Jiao, *J. Phys. Chem. C*, 2012, **118**, 7357–7362.
33 W. An, J. Fu, J. Su, L. Wang, X. Peng, K. Wu, Q. Chen, Y. Bi, B. Gao and X. Zhang, *J. Power Sources*, 2107, **345**, 227–236.
34 J. Cui, F. Cheng, J. Lin, J. Yang, K. Jiang, Z. Wen and J. Sun, *Powder Technol.*, 2017, **311**, 1–8.
35 M. Jiao, K. Liu, Z. Shi and C. Wang, *ChemElectroChem*, 2017, **4**, 542–549.
36 H. H. Li, X. L. Wu, H. Z. Sun, K. Wang, C. Y. Fan, L. L. Zhang, F. M. Yang and J. P. Zhang, *J. Phys. Chem. C*, 2015, **119**, 3495–3501.
37 X. Liu, Y. Chen, H. Liu and Z. Q. Liu, *J. Mater. Sci. Technol.*, 2016, 239–245.
38 X. Wu, Z. Q. Shi, C. Y. Wang and J. Jin, *J. Electroanal. Chem.*, 2015, **746**, 62–67.
39 H. Xia, Z. Yin, F. Zheng and Y. Zhang, *Mater. Lett.*, 2017, 205.
40 M. Sasidharan, D. Liu, N. Gunawardhana, M. Yoshio and K. Nakashima, *J. Mater. Chem.*, 2011, **21**, 13881–13888.
41 L. Ji and X. Zhang, *Electrochem. Commun.*, 2009, **11**, 1146–1149.
42 B. Guo, J. Shu, Z. Wang, H. Yang, L. Shi, Y. Liu and L. Chen, *Electrochem. Commun.*, 2008, **10**, 1876–1878.
43 A. Prasath and P. Elumalai, *ChemistrySelect*, 2016, **1**, 3363–3366.
44 J.-Y. Kim, D. T. Nguyen, J.-S. Kang and S.-W. Song, *J. Alloys Compd.*, 2015, **633**, 92–96.
45 Y.-K. Kim, J.-W. Moon, J.-G. Lee, Y.-K. Baek and S.-H. Hong, *J. Power Sources*, 2014, **272**, 689–695.
46 H. Wang, P. Wu, H. Shi, W. Tang, Y. Tang, Y. Zhou, P. She and T. Lu, *J. Power Sources*, 2015, **274**, 951–956.
47 X. Ma, Z. Wei, H. Han, X. Wang, K. Cui and L. Yang, *Chem. Eng. J.*, 2017, **323**, 252–259.